JOURNAL OF IRON AND STEEL RESEARCH, INTERNATIONAL. 2014, 21(11): 1042-1048

Dynamic Recrystallization Behavior of GCr15SiMn Bearing Steel during Hot Deformation

Dan ZHANG[1], Ya-zheng LIU[1], Le-yu ZHOU[1], Qiang HAN[1], Bo JIANG[1], Zhong-zhi LI[2]
(1. School of Material Science and Engineering, University of Science and Technology Beijing, Beijing 100083, China; 2. Dongbei Special Steel Group Corporation Limited, Dalian 116105, Liaoning, China)

Abstract: The hot deformation behavior of GCr15SiMn steel was studied through high temperature compression tests on the Gleeble-1500 thermal-mechanical simulator. The initiation and evolution of dynamic recrystallization (DRX) were investigated with microstructural analysis and then the process variables were derived from flow curves. In the present deformation conditions, the curves of strain hardening exponent (n) and the true strain (ε) at the deformation temperature of 1423 K and strain rates of 0.1, 1 and 10 s^{-1} exhibit single peak and single valley. According to Zener-Hollomon and Ludwik equation, the experimental data have been regressed by using linear method. An expression of Z parameter and hot deformation equation of the tested steel were established. Moreover, the Q values of GCr15SiMn and GCr15 steels were compared. In order to determine the recrystallization fraction under different conditions, the volume fraction of DRX as a function of process variables, such as strain rate ($\dot{\varepsilon}$), temperature (T), and strain (ε), was established. It was found that the calculated results agreed with the microstructure of the steel at any deformation conditions.

Key words: GCr15SiMn; strain hardening exponent; dynamic recrystallization; critical strain; kinetic model

During hot rolling process, dynamic recrystallization (DRX) behavior is influenced by cumulative deformation, deformation temperature and strain rate. Furthermore, the occurrence of DRX brings about deformation resistance reduction[1-4], grain refinement and mechanical properties increase[5-7]. Especially, toughness and fatigue life are affected by austenite grain size[8]. So it is of great significance to investigate the DRX behavior and austenite microstructural evolution of bearing steel during hot deformation.

In recent years, some researches on the DRX behavior of GCr15 steel have been carried out[6,9-11]. Constitutive modeling for flow behavior of GCr15 steel has been built by Yin et al[10]. Yue et al.[11] have built a mathematical model for predicting the austenite grain size in hot working of GCr15 steel. However, few investigators have focused on the DRX behavior and microstructural evolution of GCr15SiMn steel, which is a kind of high carbon chromium bearing steel with high content of Si and Mn. In the present paper, Ludwik equation and Zener-Hollomon formula will be used to analyse the variation of strain hardening exponent in different deformation stages of GCr15SiMn steel. Furthermore, a constitutive model for flow behavior of Z parameter of GCr15SiMn steel is established. The relationships between process variables (stress, strain rate and temperature) and DRX volume fraction are coupled by the modified Avrami type equation including critical strain (ε_c) and strain for maximum softening (ε^*) as a function of the temperature compensation strain rate factor during hot deformation (Z).

1 Experimental Procedure

In the present study, an electroslag smelting GCr15SiMn steel provided in the form of bar with the diameter of 150 mm is employed. The chemical composition is C 1.02%, Si 0.55%, Mn 1.07%, P

Foundation Item: Item Sponsored by National High-tech Research and Development Program (863 Program) of China (2012AA03A503)
Biography: Dan ZHANG, Doctor Candidate; **E-mail**: zdcamel@126.com; **Received Date**: June 13, 2013
Corresponding Author: Ya-zheng LIU, Doctor, Professor; **E-mail**: lyzh@ustb.edu.cn

0.006%, S 0.001%, Cr 1.49%, Cu 0.02% and Fe the balance. Before the experiment, the cylindrical specimens with the diameter of 8 mm and the length of 20 mm were machined from the hot rolled bar. To study the strain hardening behavior and DRX behavior of GCr15SiMn, the single hot compression tests were performed on a computer-controlled, servo-hydraulic Gleeble-1500 thermo-mechanical simulator. All specimens were heated to 1423 K to obtain the same initial austenite grain size. Then, they were cooled down to deformation temperatures of 1123, 1173, 1223, 1323 and 1423 K, and deformed at strain rates of 0.1, 1 and 10 s^{-1}. The specimens were quenched in water after tests immediately. The stress-strain curves under different deformation conditions were measured during deformation.

2 Results and Discussion

2.1 True stress-true strain curves and microstructure

The true stress-true strain curves for the steel tested in different deformation conditions are depicted in Fig. 1. It can be found that the effects of the deformation temperature and strain rate on the flow stress are significant in all the tested conditions. Both flow stress and peak strain increase with decreasing deformation temperature and increasing strain rate.

Fig. 2 shows a schematic diagram of stress-strain

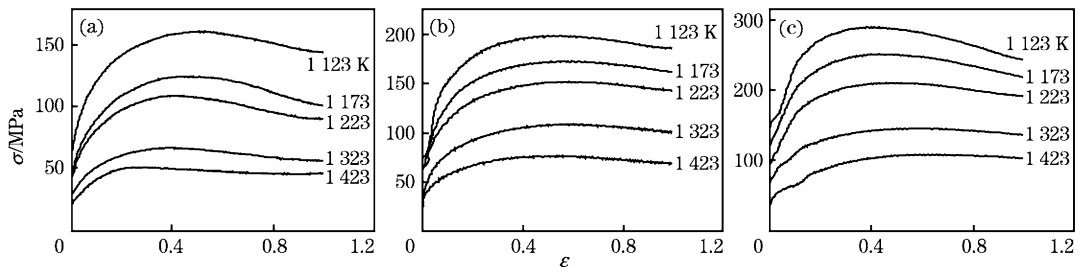

(a) 0.1 s^{-1}; (b) 1 s^{-1}; (c) 10 s^{-1}.

Fig. 1 True stress-true strain curves of GCr15SiMn steel at different deformation temperatures and strain rates

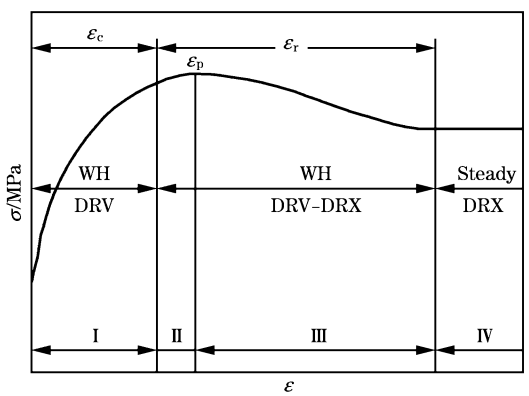

WH—Work-hardening; DRV—Dynamic recovery.

Fig. 2 Schematic diagram of the true stress-true strain curve for DRX

curve when the DRX occurs[12]. It is obvious that the flow stress obtained from experiments consists of four different stages[13], i.e., Stage I (work hardening stage), Stage II (stable stage), Stage III (softening stage) and Stage IV (steady stage).

When the strain rate is 0.1 s^{-1} and deformation temperature is from 1123 to 1423 K, the flow stress increases rapidly with increasing true strain. As the critical strain ε_c is smaller than ε_r, which terms as the necessary strain to finish DRX, the DRX is in a stable deformation (Fig. 2). However, with continuous deformation, strain of new DRX grains reaches ε_c again, the DRX will occur for the second round. Also, DRX will occur repeatedly in austenite grains during deformation, and each grain may be in different stages of DRX. Finally, it will get to the stable deformation stage of DRX when the work hardening corresponds to the dynamic softening.

The true stress-true strain curves of the steel immediately arrived at steady state region when deformed at 1 s^{-1} and 1123—1423 K. At 10 s^{-1}, peak stress does not arrive at steady state region but still in the decreasing stage although the true stress reached 1.0. It demonstrates that the effect of dynamic softening is stronger than that of work hardening, and it is in partly DRX stage when the true strain is 1.0.

Fig. 3 shows the central microstructures of specimens deformed at 1 s^{-1} and various temperatures (1123, 1173, 1223 and 1423 K). The comparison displays that partly DRX occurred when deformed at 1123 and 1173 K. While deformed temperature is greater than 1223 K, the occurrence of the complete DRX in the specimens can be certified. The process of DRX will be accelerated with increasing deformation temperature and decreasing strain rate.

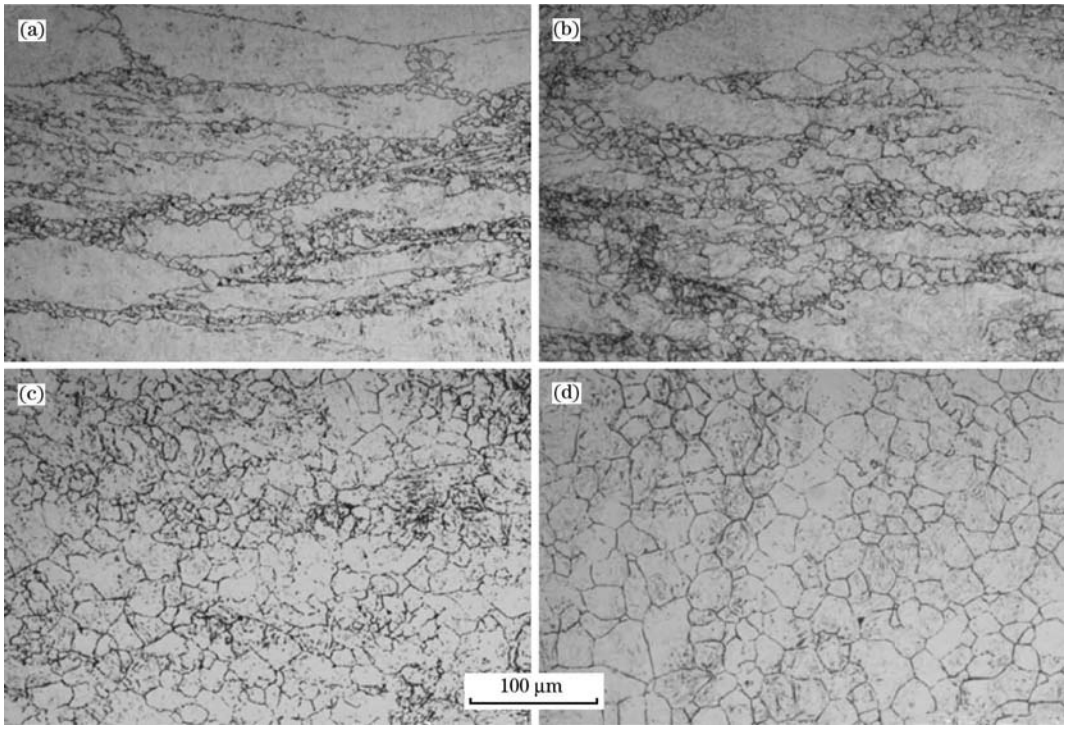

(a) 1 s^{-1}, 1123 K; (b) 1 s^{-1}, 1173 K; (c) 1 s^{-1}, 1223 K; (d) 1 s^{-1}, 1423 K.

Fig. 3 Optical microstructure after hot deformation

2.2 Work hardening characteristic in hot deformation

In the hot compression process of tested steel, work hardening behavior occurs accompanied with dynamic softening behavior such as dynamic recovery and dynamic recrystallization. True stress-true strain curves are able to show overall trend of stress changes but limited to reflect the deformation mechanism sensitively. Therefore, the change rule of strain hardening exponent in different stages is analysed by Ludwik equation[14] and Crussard-Jaoul analysis[15].

The Ludwik relation is expressed as:

$$\sigma=\sigma_0+K\varepsilon^n \quad (1)$$

where, σ_0 is yeild strength; K is material constants and n is strain hardening exponent. The strain hardening rate θ, which is obtained from the differential form of Eq. (1) with respect to ε, is expressed as:

$$\theta=\mathrm{d}\sigma/\mathrm{d}\varepsilon=Kn\varepsilon^{n-1} \quad (2)$$

The logarithmic form of Eq. (2) is:

$$\ln(\mathrm{d}\sigma/\mathrm{d}\varepsilon)=\ln K+\ln n+(n-1)\ln\varepsilon \quad (3)$$

According to the Hollomon equation and Eq. (3), curves of n-ε (Fig. 4) and Crussard-Jaoul analysis (Fig. 5) are plotted with deformation temperature of 1 423 K and strain rates of 0.1, 1, and 10 s^{-1} based on the experimental data.

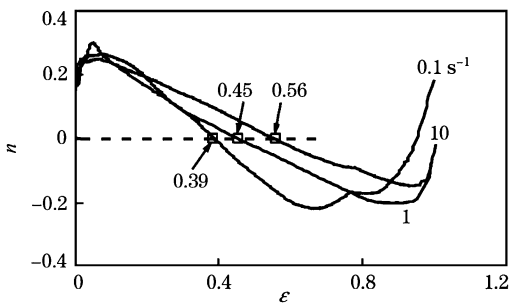

Fig. 4 Relationships between n and ε at deformation temperature of 1 423 K

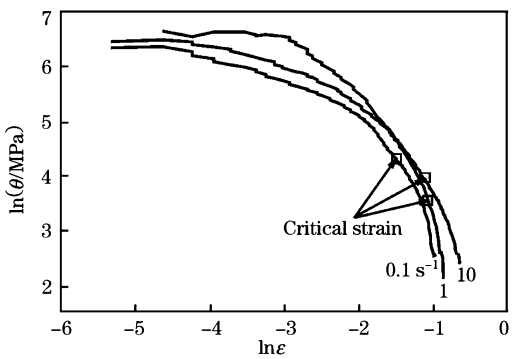

Fig. 5 Curves of C-J (Crussard-Jaoul) analysis at deformation temperature of 1 423 K

At the beginning of deformation, n value increases with increasing true strain. When deformed at strain rates of 10, 1 and 0.1 s^{-1}, the peak values in n-ε curves are 0.30, 0.25 and 0.26 respectively, corresponding to the true strains of 0.0488, 0.0732

and 0.0830. However, the peak value corresponds to less strain and the value is larger when strain rate is 10 s^{-1}. The peak values at strain rates of 0.1 and 1 s^{-1} are close. It is attributed to the formation of high density dislocation networks and dislocation walls, which are caused by strong dislocation multiplication and delivery at high strain rate. In addition, dislocation movements are restrained by lattice defects, and it will become stronger and stronger with increasing true strain[16], consequently, n value will become larger and larger.

Moreover, it will take less time to experience the same deformation in high strain rate condition than in low strain rate condition. So, the dynamic softening behavior such as the combination and rearrangement of dislocations and the dynamic recovery, progresses insufficiently, which makes a higher n value. When the true strain gets to the critical strain of DRX of each curve (Fig. 5), the DRX will occur and the n values begin to descend. As the true strains increase to 0.39, 0.45 and 0.56 at strain rates of 0.1, 1 and 10 s^{-1} respectively, the effect of strain hardening and dynamic softening is equivalent and the n values equal to zero. With increasing the true strains, the n values corresponding to the valley strains are −0.22, −0.20 and −0.15 respectively. After that, n values increase for the second time. This is attributed to the increase of new dislocations generated in the DRX grains with the increase of true strains.

2.3 Constitutive equation of flow stress for GCr15SiMn steel

It is known that the softening mechanism is controlled by the thermally activated stored energy developed during deformation, which induces different DRX softening and work-hardening. The activation energy of DRX determines the critical conditions for DRX initiation. To further investigate the hot deformation behaviors of GCr15SiMn steel, it is necessary to study the constitutive characteristics. The Arrhenius equation is widely used to describe the relationship between the strain rate, flow stress and temperature, especially at high temperature. It can also be formulated by Zener-Hollomon parameter Z in an exponent-type equation as shown in following equation[17,18]:

$$Z=\dot{\varepsilon}\exp[Q/(RT)] \tag{4}$$

It can also be expressed as:

$$Z=\begin{cases}A\sigma_p^{n_0} & \sigma\beta/n_0<0.8\\ B\exp(\beta\sigma_p) & \sigma\beta/n_0>1.2\end{cases} \tag{5}$$

where, Z is the temperature compensation strain rate factor during hot deformation; A, B, β and n_0 are material constants; $\dot{\varepsilon}$ is strain rate, s^{-1}; Q the activation energy of hot deformation, kJ·mol^{-1}; R is the universal gas constant, 8.314 J·mol^{-1}·K^{-1} and T is the absolute temperature, K. If there is no peak stress (σ_p), σ_p is replaced by σ_s.

Sellars and Tegart[19] confirm that the function among stable flow stress, strain rate, and temperature can be expressed more suitably by the Arrhenius relationship modified by hyperbolic sine function:

$$Z=\dot{\varepsilon}\exp[Q/(RT)]=C[\sinh(\alpha\sigma_p)]^{n'} \tag{6}$$

where, C, α and n' are constants. The relationship among α, β and n_0 is $\alpha=\beta/n_0$. From Eqs. (4) and (5), Eq. (7) can be obtained,

$$\dot{\varepsilon}\exp[Q/(RT)]=B\exp(\beta\sigma_p) \tag{7}$$

Taking the logarithm of both sides of Eq. (7) gives

$$\sigma_p=\ln\dot{\varepsilon}/\beta+Q/(\beta RT)-\ln B/\beta \tag{8}$$

Then, at constant temperature, substituting the values of the peak stress and corresponding strain rate into Eq. (8) gives the relationship between the peak stress and strain rate (Fig. 6(a)). It shows that the peak stresses can be approximated by a group of parallel and straight lines in the hot deformation conditions. The values of β can be obtained by Eq. (8) from the slope of the lines in the σ_p-$\ln\dot{\varepsilon}$ plots. In the same way, at constant strain rate, the values of Q can be obtained by Eq. (8) from the slope of the lines in the σ_p-T^{-1} plots. The mean values of β and Q can be computed as 0.0553 MPa^{-1} (Fig. 6(a)) and 304.056 kJ·mol^{-1} (Fig. 6(b)), respectively. Substitute β and Q into Eq. (8), then B can be computed as 2.304×10^9.

Substituting the value of Q into Eq. (4), Zener-Hollomon parameter for GCr15SiMn steel can be represented as follows:

$$Z=\dot{\varepsilon}\exp[304056/(RT)]=C[\sinh(\alpha\sigma_p)]^{n'} \tag{9}$$

Combining Eqs. (4) and (5) gives

$$\dot{\varepsilon}\exp[Q/(RT)]=A\sigma_p^{n_0} \tag{10}$$

Taking the logarithm of both sides of Eq. (10) gives

$$\ln\sigma_p=\ln\dot{\varepsilon}/n_0-\ln A/n_0+Q/(n_0RT) \tag{11}$$

In the same way, the value of n_0 can be obtained from the slope of the lines in the $\ln\sigma_p$-$\ln\dot{\varepsilon}$ plots. As the slope of the lines is approximately the same, the value of n_0 can be obtained for different deformation temperatures by linear fitting method, and a mean value of n_0 can be computed as 6.550 (Fig. 7). Then

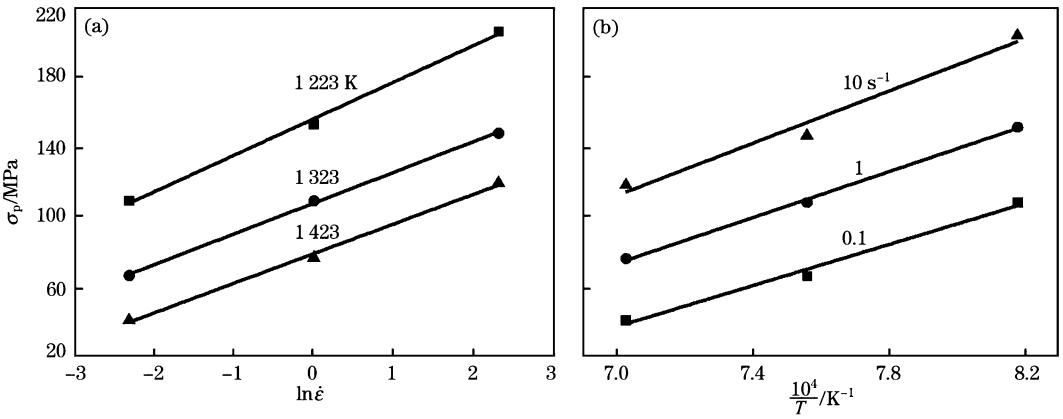

Fig. 6 Relationships between peak stress and deformation parameters

A can be fitted by Eq. (10) and is approximately 0.070. So $\alpha=\beta/n_0=0.00844$ MPa^{-1}.

Taking the logarithm of both sides of Eq. (6) gives

$$\ln\dot{\varepsilon}=\ln C+n'\ln[\sinh(\alpha\sigma_p)]-Q/(RT) \quad (12)$$

A mean value of n' and C fitted from Eq. (12) are 4.700 and 1.008×10^{12} respectively (Fig. 8).

Finally, substituting the values of α, n', C and Q into Eq. (9), the peak stress constitutive equation of hot deformation for GCr15SiMn steel can be expressed as follows:

$$\dot{\varepsilon}=1.008\times10^{12}[\sinh(0.00844\sigma_p)]^{4.7}\times\exp[-304056/(RT)] \quad (13)$$

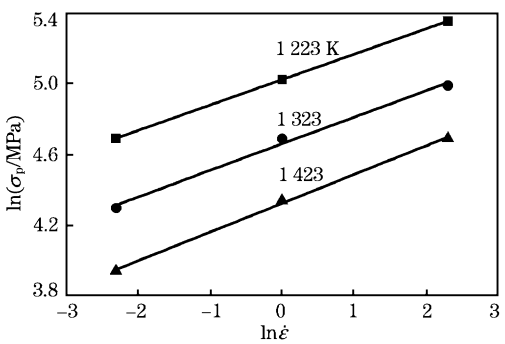

Fig. 7 Relationships between lnσ_p and ln$\dot{\varepsilon}$

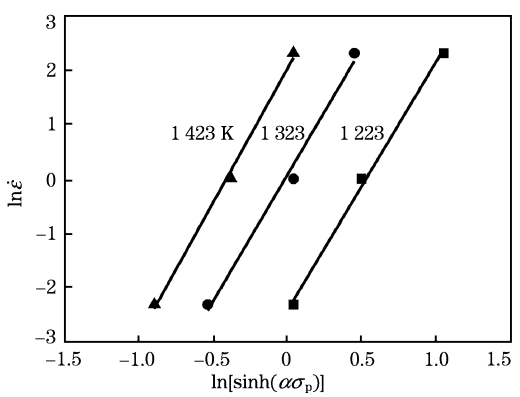

Fig. 8 Relationships between ln$\dot{\varepsilon}$ and ln[sinh($\alpha\sigma_p$)]

Also, Zener-Hollomon parameter for GCr15SiMn steel can be represented as follows:

$$Z=\dot{\varepsilon}\exp[304056/(RT)]=1.008\times10^{12}\times[\sinh(0.00844\sigma_p)]^{4.7} \quad (14)$$

In the study of Yue et al. [6] and Yin et al. [10] about the flow behavior of GCr15 steel, the hot deformation activation energies are 351 and 439 kJ/mol, respectively, while the Q value is 304.056 kJ/mol in this study.

Compared with GCr15 steel in Ref. [6] and GCr15SiMn steel in this study, the mass percents of Si and Mn are 0.24% and 0.55%, 0.36% and 1.07% respectively. Li et al. [20] have studied the influence of Mn content on dynamic recrystallization of ferrite in low carbon steels. It shows that the increase of Mn content in low carbon steel is unfavorable for the progress of dynamic recrystallization of ferrite. However, under the deformation condition that the progress of dynamic recrystallization of ferrite can occur completely, the increase of Mn content can promote the progress of dynamic recrystallization. In this study, the increase of Si and Mn contents in high-carbon chromium steel reduces the hot deformation activation energy and promotes the progress of dynamic recrystallization, which is probably due to that Si and Mn can accelerate the nucleation of dynamic recrystallization.

2.4 DRX kinetic model

From the critical strain, at which DRX is initiated to steady state strain, new grains are formed at deformation bands and grain boundaries of original austenite grains. During the following deformation, the dislocations multiplication caused by deformation and the dislocations disappearance caused by DRX are concomitant. When the effects of strain hardening and dynamic softening are dynamically balanced, flow stress keeps constant with the increase of strain,

and the DRX grains have equiaxed shape and keep constant size[6,21-25]. The kinetics of DRX can be described in terms of normal S-curves which can be expressed as a function of time. In constant strain rates, time can be replaced by strain and the recrystallized fraction can be described by Avrami equation[24,25]. Thus, the evolution of microstructure after DRX can be predicted by the following equation:

$$X_{DRX}=1-\exp\{-[(\varepsilon-\varepsilon_c)/\varepsilon^*]^m\} \quad (15)$$

where, X_{DRX} is the volume fraction of dynamically recrystallized grain; m is the Avrami's constant; ε_c is critical strain and ε^* is the strain for maximum softening. The expression is modified from the Avrami's equation. It indicates that X_{DRX} depends on the strain and other deformation conditions.

The data of true stress-true strain curve after the peak stress point were used to calculate DRX softening rate ($\theta=d\sigma/d\varepsilon$ versus σ) plots (Fig. 9). The maximum softening rate corresponds to the negative peak of such plot. The critical strain and the strain for maximum softening rate could be considered with a function of dimensionless parameter Z/A (Fig. 10). The function expressions linearly fitted by the method of least squares are $|\varepsilon^*|=0.77168(Z/C)^{0.07474}$ and $|\varepsilon_c|=0.34561(Z/C)^{0.05702}$.

m is identified with a hypothesis $X_{DRX}=1$. It means

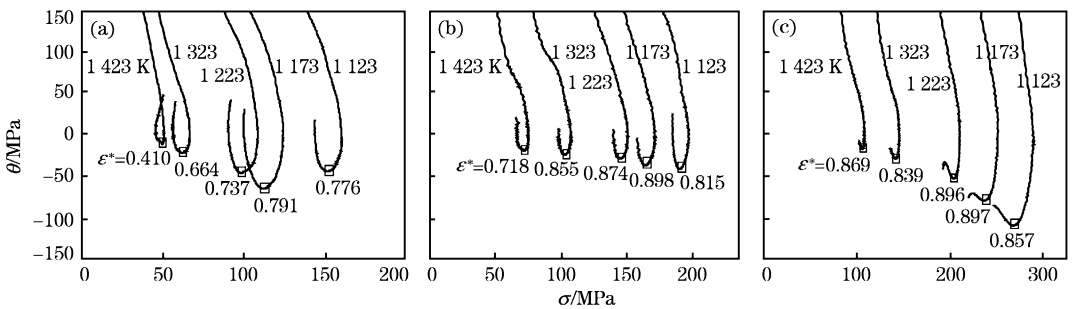

(a) 0.1 s^{-1}; (b) 1 s^{-1}; (c) 10 s^{-1}.

Fig. 9 Plots of θ ($d\sigma/d\varepsilon$) versus σ after the peak points of the true stress-true strain curves at different deformation temperatures and strain rates

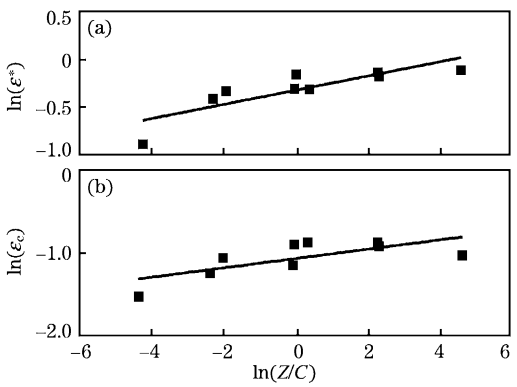

Fig. 10 Relationship between the dimensionless parameters

that the flow stress reaches a steady state, and the complete DRX grains have equiaxed shape and keep constant size. From the true compressive stress-true strain curves (Fig. 1) and θ versus σ plots (Fig. 9), such deformation conditions can be identified as shown in Table 1. Substituting these deformation conditions corresponding to $X_{DRX}=1$ into Eq. (14), the mean value of m can be obtained as 8.13913. Thus, the kinetic model of DRX calculated from true compressive stress-strain curves can be expressed as Table 2.

Table 1 Deformation strain corresponding to $X_{DRX}=1$

ε	T/K	$\dot{\varepsilon}/s^{-1}$
0.94—1.00	1223	0.1
0.83—1.00	1323	0.1
0.64—1.00	1423	0.1
0.89—1.00	1323	1
0.71—1.00	1423	1

Table 2 Kinetic model of DRX calculated from true compressive stress-strain curves

Volume fraction of dynamically recrystallized grain	Exponent
$X_{DRX}=1-\exp\{-[(\varepsilon-\varepsilon_c)/\varepsilon^*]^m\}$	$\lvert\varepsilon^*\rvert=0.77168(Z/C)^{0.07474}$ $\lvert\varepsilon_c\rvert=0.34561(Z/C)^{0.05702}$ $Z=\dot{\varepsilon}\exp[304056/(RT)]$ $C=1.008\times10^{12}$ $m=8.3194$

The effect of deformation conditions on the volume fraction of DRX according to the calculation results of this model is shown in Fig. 11. It shows that with the increase of true strain, the volume fraction of DRX increases and reaches a constant value of 100%, which means the completion of DRX process.

The DRX is thermally activated so that the X_{DRX} increased with temperature for a specific strain rate. However, for a fixed temperature, the X_{DRX} decreased with strain rate. This effect can be attributed to decreased mobility of grain boundaries (growth kinetics) with increasing strain rate and decreasing temperature[5]. Thus, higher strain rates and lower temperatures delay the occurrence of DRX as metal deforming.

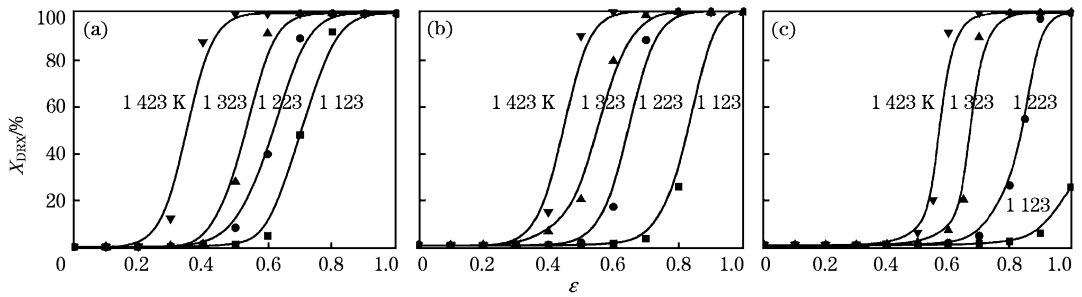

(a) 0.1 s^{-1}; (b) 1 s^{-1}; (c) 10 s^{-1}.

Fig. 11 Predicted volume fractions of dynamic recrystallization obtained at different deformation temperatures and strain rates

3 Conclusions

(1) In the present deformation conditions of GCr15SiMn steel, the curves of strain hardening exponent and the true strain at deformation temperature of 1423 K have single peak and single valley at strain rates of 0.1, 1 and 10 s^{-1}. During the work-hardening process, dislocation strengthening is the major work-hardening mechanisms of the tested steel.

(2) By means of least square method, the experimental data are regressed by using linear method. Q and n' are obtained to be 304.056 kJ/mol and 4.700, respectively, and $Z=\dot{\varepsilon}\exp[304056/(RT)]=1.008\times10^{12}[\sinh(0.00844\sigma_p)]^{4.7}$. The peak stress constitutive equation of hot deformation for GCr15SiMn steel is $\dot{\varepsilon}=1.008\times10^{12}[\sinh(0.00844\sigma_p)]^{4.7}\exp[-304056/(RT)]$.

(3) The increase of Si and Mn contents in high-carbon chromium steel reduces the hot deformation activation energy and promotes the progress of dynamic recrystallization.

(4) The strain for maximum softening rate and the critical strain were described by the functions of dimensionless parameter, Z/A. The evolution of DRX volume fraction was characterized by the modified Avrami type equation including the parameters Q, Z/A, ε_c and ε^*.

References:

[1] S. H. Cho, S. I. Kim, Y. C. Yoo, Met. Mater. Int. 4 (1998) 732-736.
[2] S. H. Cho, S. I. Kim, Y. C. Yoo, J. Mater. Sci. Lett. 16 (1997) 1836-1837.
[3] E. I. Poliak, J. J. Jonas, Acta Mater. 44 (1996) 127-136.
[4] C. Roucoules, P. D. Hodgson, S. Yue, J. J. Jonas, Metall. Mater. Trans. A 25 (1994) 389-400.
[5] G. Z. Quan, G. S. Li, T. Chen, Y. X. Wang, Y. W. Zhang, J. Zhou, Mater. Sci. Eng. A 58 (2011) 4643-4651.
[6] C. X. Yue, L. W. Zhang, S. L. Liao, J. B. Pei, H. J. Gao, Y. W. Jia, X. J. Lian, Mater. Sci. Eng. A 499 (2009) 177-181.
[7] Y. C. Lin, M. S. Chen, J. Zhang, Mater. Sci. Eng. A 499 (2009) 88-92.
[8] H. K. D. H. Bhadeshia, Prog. Mater. Sci. 57 (2012) 268-435.
[9] S. D. Gu, L. W. Zhang, C. X. Yue, J. H. Ruan, J. L. Zhang, H. J. Gao, Comput. Mater. Sci. 50 (2011) 1951-1957.
[10] F. Yin, L. Hua, H. J. Mao, X. H. Han, Mater. Des. 43 (2012) 393-401.
[11] C. X. Yue, L. W. Zhang, S. L. Liao, H. J. Gao, Comput. Mater. Sci. 45 (2009) 462-466.
[12] R. Ebrahimi, S. Zahiri, A. Najafizadeh, J. Mater. Process. Technol. 17 (2006) 301-305.
[13] Y. C. Lin, M. S. Chen, J. Zhong, Comput. Mater. Sci. 42 (2008) 470-477.
[14] R. E. Reed-Hill, W. R. Cribb, S. N. Monteiro, Metall. Trans. 4 (1973) 2665-2667.
[15] C. Crussard, Rev. Metall. 10 (1953) 697-701.
[16] R. B. Song, J. Y. Xiang, D. P. Hou, Acta Metall. 46 (2010) 57-61.
[17] H. J. McQueen, Mater. Sci. Eng. A 322 (2002) 345-362.
[18] K. Karhausen, R. Kopp, Steel Res. Int. 63 (1992) 247-256.
[19] C. M. Sellars, W. J. M. Tegart, Mem. Sci. Rev. Met. 63 (1966) 731-736.
[20] L. F. Li, W. Y. Yang, Z. Q. Sun, Acta Metall. 40 (2004) 1257-1263.
[21] S. I. Kim, Y. C. Yoo, Mater. Sci. Eng. A 311 (2001) 108-113.
[22] G. L. Ji, F. G. Li, Q. H. Li, H. Q. Li, Z. Li, Mater. Sci. Eng. A 527 (2010) 2350-2355.
[23] D. Ponge, G. Gottstein, Acta Mater. 46 (1998) 69-80.
[24] S. F. Medina, C. A. Hernandez, Acta Mater. 44 (1996) 149-154.
[25] J. Cabrera, A. Al Omar, J. Prado, J. Jonas, Metall. Mater. Trans. A 28 (1997) 2233-2244.